Direct versus indirect band gap emission and exciton-exciton annihilation in atomically thin molybdenum ditelluride ($MoTe_2$)

Guillaume Froehlicher, Etienne Lorchat, and Stéphane Berciaud*

Institut de Physique et Chimie des Matériaux de Strasbourg and NIE, UMR 7504, Université de Strasbourg and CNRS, 23 rue du Læss, BP43, 67034 Strasbourg Cedex 2, France

(Received 9 February 2016; revised manuscript received 19 July 2016; published 26 August 2016)

We probe the room temperature photoluminescence of N-layer molybdenum ditelluride ($MoTe_2$) in the continuous wave (cw) regime. The photoluminescence quantum yield of monolayer $MoTe_2$ is three times larger than in bilayer $MoTe_2$ and 40 times greater than in the bulk limit. Mono- and bilayer $MoTe_2$ display almost symmetric emission lines at 1.10 and 1.07 eV, respectively, which predominantly arise from direct radiative recombination of the A exciton. In contrast, $N \geqslant 3$-layer $MoTe_2$ exhibits a much reduced photoluminescence quantum yield and a broader, redshifted, and seemingly bimodal photoluminescence spectrum. The low- and high-energy contributions are attributed to emission from the indirect and direct optical band gaps, respectively. Bulk $MoTe_2$ displays a broad emission line with a dominant contribution at 0.94 eV that is assigned to emission from the indirect optical band gap. As compared to related systems (such as MoS_2, $MoSe_2$, WS_2, and WSe_2), the smaller energy difference between the monolayer direct optical band gap and the bulk indirect optical band gap leads to a smoother increase of the photoluminescence quantum yield as N decreases. In addition, we study the evolution of the photoluminescence intensity in monolayer $MoTe_2$ as a function of the exciton formation rate W_{abs} up to 3.6×10^{22} cm^{-2} s^{-1}. The line shape of the photoluminescence spectrum remains largely independent of W_{abs}, whereas the photoluminescence intensity grows sublinearly above $W_{abs} \sim 10^{21}$ cm^{-2} s^{-1}. This behavior is assigned to exciton-exciton annihilation and is well captured by an elementary rate equation model.

DOI: 10.1103/PhysRevB.94.085429

I. INTRODUCTION

Transition metal dichalcogenides [1] (herein denoted MX_2, where M = Mo, W, Re and X = S, Se, Te) are an actively investigated class of layered materials, whose basic electronic, optical, and vibrational properties depend critically on the number of layers N that compose a given sample [2–6]. N-dependent properties are remarkably illustrated by the transition from indirect optical band gap, in the bulk form, to direct optical band gap [7] at monolayer thickness that occurs in $2Hc$ Mo- and W-based semiconducting MX_2 [2,3,8–11]. Direct optical band gaps, together with the possibility of achieving valley polarization for resonantly pumped band-edge excitons in monolayer MX_2 [12], open original perspectives for two-dimensional (2D) optoelectronics [13] and valleytronics [14].

An interesting direction in this field, consists in exploring MX_2 with smaller optical band gaps (i.e., related to the formation of tightly bound excitons [15–23]) than the extensively studied monolayers of MoS_2, $MoSe_2$, WS_2, WSe_2, whose optical band gaps lie in the range 1.5–2.0 eV [23]. Such endeavors are motivated by the possibility of achieving gate-controlled ambipolar transport more easily [24,25] and to extend optoelectronic applications of MX_2 and related van der Waals heterostructures [26] into the near-infrared range. Among possible candidates, N-layer molybdenum ditelluride ($MoTe_2$) [6,24,25,27–33], as well as rhenium diselenide ($ReSe_2$), have emerged very recently. While N-layer $ReSe_2$ crystals exhibit a distorted $1T$ phase [34–37] and are indirect optical band gap semiconductors, irrespective of N [35], stable N-layer $2Hc$-$MoTe_2$ crystals have been shown to undergo a transition from indirect (for bulk $MoTe_2$) to direct (for monolayer $MoTe_2$) optical band gap [27,28]. However, the exact value of N at which the crossover occurs is a matter of debate [28] and a detailed analysis of the photoluminescence (PL) line shape in N-layer $MoTe_2$ is still lacking. In addition, the evolution of the PL spectrum and integrated PL intensity of monolayer $MoTe_2$ with increasing exciton density remains unexplored so far.

In this article we address the room temperature PL properties of N-layer $2Hc$-$MoTe_2$ in the continuous wave (cw) regime. Our data show that the PL quantum yield of monolayer $MoTe_2$ is approximately three times (40 times) larger than that of bilayer (bulk) $MoTe_2$, confirming the transition from a bulk indirect optical band gap (giving rise to an emission line at 0.94 eV) to a direct optical band gap at 1.10 eV [27]. Moreover, an analysis of the PL line shapes reveals two close-lying contributions to the PL spectra. For mono- and bilayer $MoTe_2$, the observation of similar, almost symmetric PL spectra indicates that the crossover from dominant indirect to dominant direct band gap emission presumably occurs between $N = 3$ and $N = 2$ at room temperature. For $N = 3$ to $N = 7$ layers $MoTe_2$, the low- and high-energy PL features are assigned to emission from the indirect and direct optical band gaps, respectively. Finally, the PL intensity of monolayer $MoTe_2$ levels off with increasing laser intensity (i.e., as the exciton formation rate increases). This nonlinear behavior unveils the critical role of exciton-exciton annihilation in atomically thin $MoTe_2$, as also reported recently in other MX_2 [22,38–42].

II. METHODS

N-layer crystals of trigonal prismatic ($2Hc$ phase) $MoTe_2$ [hereafter denoted $MoTe_2$, see Fig. 1(a)] were prepared by mechanical exfoliation of commercially available bulk crystals (2D semiconductors) onto Si wafers covered with a 90-nm-thick SiO_2 epilayer [see Fig. 1(b)]. The number of layers was

*stephane.berciaud@ipcms.unistra.fr

first estimated from optical contrast and further confirmed by ultralow-frequency micro-Raman spectroscopy [see Figs. 1(c) and 1(d)]. PL and Raman spectra were recorded in ambient conditions, both in a backscattering geometry, using a home-built setup. In Raman experiments, a combination of one narrow bandpass filter and two narrow notch filters (Optigrate) was used in order to attain the low-frequency range of the spectrum. After optimization, Raman features at frequencies as low as 4.5 cm^{-1} could be measured [see Fig. 1(c)]. In all experiments, freshly prepared samples [31] were optically excited using a single longitudinal mode, linearly polarized, 2.33 eV (532 nm) laser beam focused onto a $\approx$ 600-nm-diameter spot using a high numerical aperture objective (NA = 0.65). PL spectra in Figs. 2 and 3 were recorded in the linear regime at a laser intensity of approximately 1.5 kW/cm^2, using a single monochromator equipped with a 150 grooves/mm ruled grating coupled to a thermoelectrically cooled two-dimensional InGaAs array (Princeton Instruments NIRvana). Raman spectra were recorded at a laser intensity of approximately 60 kW/cm^2, using the same monochromator equipped with a 2400 grooves/mm holographic grating, coupled to a two-dimensional liquid nitrogen cooled charge-coupled device (CCD) array. We have verified that the higher laser intensities employed for Raman studies were not damaging our samples.

III. DETERMINATION OF THE NUMBER OF LAYERS N

Figure 1(c) shows the low-frequency Raman spectra (in the range 0–40 cm^{-1}) of N-layer $MoTe_2$, from $N = 1$ to $N = 7$, and of a thick sample ($N \gtrsim 50$ layers) considered as a bulk reference. As previously reported [6], the low-energy features observed for $N \geqslant 2$ correspond to *interlayer* shear (LSM) and breathing (LBM) modes [see the gray dashed lines in Fig. 1(c)]. In bulk $MoTe_2$, the LBM is silent [43,44] and only a single peak, assigned to the LSM, can be observed. The evolution of the LSM and LBM frequencies with N can be analytically described by the expression $\omega_k(N) = \frac{\omega_0}{\sqrt{2}}\sqrt{1-\cos(\frac{k\pi}{N})}$ (with $k = 1,\ldots,N-1$) deduced from a finite linear chain model [6,44–47]. Using this expression, the observed modes were fit using $k = N - 1$ for the LSM branch (Sa) and $k = 1,3,5$ for the LBM branches (Ba, Bb, and Bc, respectively), as shown in Fig. 1(d). These fits yield bulk frequencies $\omega_0^{LSM} = 26.8$ cm^{-1} and $\omega_0^{LBM} = 39.9$ cm^{-1} in excellent agreement with the results in Ref. [6], further confirmed in Refs. [48,49]. This analysis permits an unambiguous determination of N.

IV. PL SPECTRA OF N-LAYER $MoTe_2$

Figure 2(a) displays the raw PL spectra of the $MoTe_2$ samples ($N = 1$ to $N = 7$ and bulk) previously introduced in Fig. 1. It is well known that interference effects strongly affect the exciton formation rate, as well as the Raman [50,51] and PL [52] response of layered materials deposited on layered substrates such as Si/SiO_2. In order to take these phenomena into account, *interference-free* PL spectra were obtained by normalizing the raw spectra by the enhancement factor calculated following Refs. [50,51] (see Fig. 2(b) and the Supplemental Material [53]). This procedure allows us

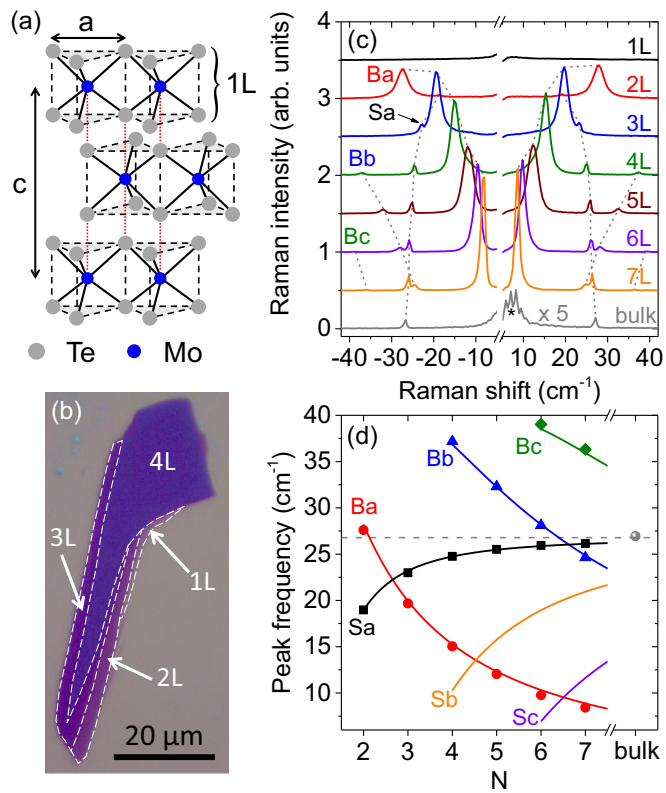

FIG. 1. (a) Side view of the crystal structure of $2Hc$-$MoTe_2$. (b) Optical image of a $MoTe_2$ flake (deposited onto a Si/SiO_2 substrate) containing mono- to tetralayer domains. The boundaries of the various layers are highlighted with dashed lines. (c) Ultralow-frequency Raman spectra of $N = 1$ to $N = 7$ layer $MoTe_2$ and of bulk $MoTe_2$. The asterisk highlights residual contributions from the exciting laser beam. (d) Fan diagram of the interlayer shear (Sa, Sb, and Sc) and breathing (Ba, Bb, and Bc) modes of $MoTe_2$. Symbols are frequencies extracted from the Raman spectra in (c). The solid lines are theoretical calculations based on a linear chain model and the gray dashed line corresponds to the bulk frequency of the interlayer shear mode.

to compare, in Fig. 2(c), the interference-free PL quantum yields, which are proportional to the integrated intensity of the interference-free PL spectra. Note that the enhancement factor takes into account the number of layers and is thus homogeneous to a length. Therefore, the interference-free PL quantum yields are given per unit length. Moreover, contrary to what was reported in Ref. [29], the PL background from the Si substrate is negligible in our experiments (see Supplemental Material [53]).

Figure 2(b) displays the interference-free PL spectra. The PL line shapes are marginally affected as compared to the raw spectra, whereas the integrated interference-free PL intensities are significantly modified. As N increases, we immediately notice that (i) the integrated PL intensity decreases monotonically and is three (40) times smaller in bilayer (bulk) $MoTe_2$ than in the monolayer limit [see Fig. 2(c)], (ii) the PL peak energy redshifts from 1.10 eV at monolayer thickness down to 0.94 eV in the bulk limit, and (iii) the PL line shapes are slightly asymmetric for $N = 1,2$ and clearly bimodal for $N \geqslant 3$. The first two observations are consistent with a transition from an

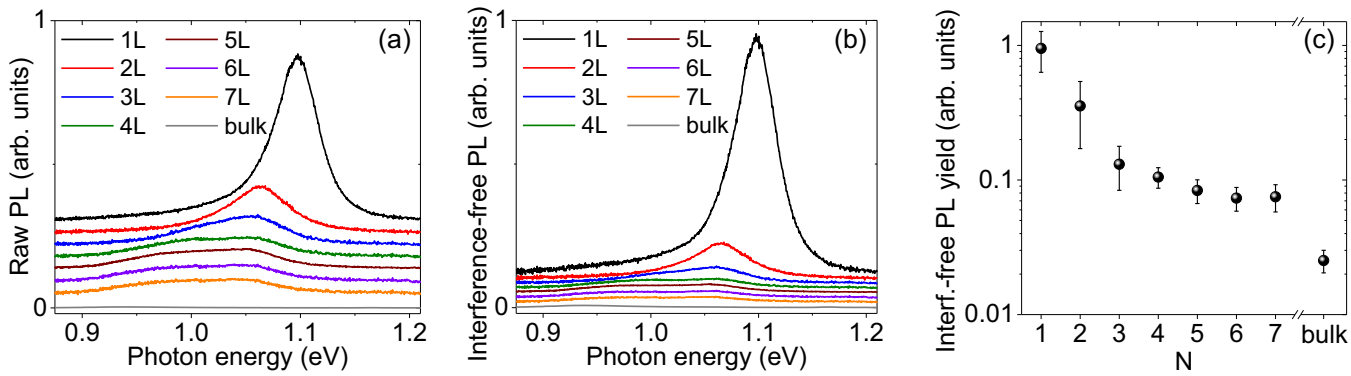

FIG. 2. (a) Raw and (b) interference-free photoluminescence spectra of $N = 1$ to $N = 7$ layer $MoTe_2$ and of bulk $MoTe_2$ deposited on a Si/SiO_2 substrate. (c) Average total integrated intensities of the interference-free photoluminescence spectra as a function of N obtained on three samples (except for $N = 5$ and $N = 6$, for which only one sample was studied).

indirect optical band gap in the bulk limit to a direct optical band gap for $N = 1$ [27]. The increase in PL quantum yield as N decreases is moderate, as compared to recent observations in MoS_2, $MoSe_2$, WS_2, and WSe_2 [2,9,10]. This behavior is due to the smaller energy difference between the bulk emission from the indirect optical band gap and the direct optical band gap. For instance, the latter is approximately 0.6 eV in MoS_2 [2] and 0.5 eV in $MoSe_2$ [9].

V. INDIRECT-TO-DIRECT OPTICAL BAND GAP CROSSOVER

The exact value of N at which the crossover occurs is still debated. At room temperature, Ruppert *et al.* [27] have suggested a crossover when reaching the monolayer limit, while at low temperature (4–180 K), Lezama *et al.* [28] concluded that the crossover occurs between $N = 3$ and $N = 2$. Very recently, at 10 K, Robert *et al.* [54] have observed similar PL intensities in mono- and bilayer $MoTe_2$ and a slightly longer PL decay time in bilayer $MoTe_2$ than in monolayer $MoTe_2$, suggesting that PL in bilayer $MoTe_2$ may in part originate from the direct optical band gap. However, there is no apparent contradiction between these claims since it is well known that temperature might affect the crossover [8]. Here we could clearly identify two subfeatures within each PL spectrum, as illustrated in Fig. 3. We may now wonder whether these two contributions may be associated with the direct and indirect optical band gaps. To answer this question, we have systematically fit the PL spectra with a double Voigt profile (see Fig. 3) and extracted the high- (PL^+) and low-energy (PL^-) contributions. Figure 4 displays the peak positions PL^+_{max} and PL^-_{max}.

First, the PL spectrum of monolayer $MoTe_2$ exhibits an almost symmetric line shape dominated by a relatively narrow PL^+ feature with a full width at half maximum (FWHM) of approximately 50 meV. The peak position PL^+_{max} matches the energy of the A exciton measured by room temperature differential reflectance spectroscopy by Ruppert *et al.* [27] [see Fig. 4(a)] and PL^+_{max} is therefore identified as the direct optical band gap energy. The PL^- shoulder is much broader (FWHM of approximately 100 meV) and has lower integrated intensity than that of the PL^+ peak. Assuming that monolayer $MoTe_2$ is a direct optical band gap semiconductor, the PL^- feature cannot arise from the indirect optical band gap. Since the energy difference between the $PL^\pm$ features is approximately 30 meV [see Fig. 4(b)], the PL^- peak can tentatively be assigned to emission from charged A excitons (i.e., trions [28,29]) or to exciton-phonon sidebands involving coupling of A excitons with Γ-point optical phonons (whose energies lie in the range 15–35 meV [6,30]).

Second, the PL spectrum of bilayer $MoTe_2$ is slightly redshifted (by about 30 meV) with respect to the monolayer case, with a normalized PL quantum yield about three times smaller than that of monolayer $MoTe_2$, suggesting that bilayer $MoTe_2$ is not a direct optical band gap semiconductor. However, although the bilayer PL spectrum is appreciably broader than that of the monolayer PL spectrum (FWHM of approximately 65 meV), the spectra are similar. Indeed, PL^+_{max} also matches the energy of the A exciton for $N = 2$ [27]. In addition, the PL^+ peak is more intense than the PL^- peak, and the energy difference between the peak positions of these two features remains approximately 30 meV (see Fig. 4), as in monolayer $MoTe_2$. These observations indicate that the room temperature PL in mono- and bilayer $MoTe_2$ likely originates from similar mechanisms. However, the reduced PL quantum yield of bilayer $MoTe_2$ suggests that the indirect optical band gap is slightly smaller than the direct optical band gap such that phonon-assisted emission across the indirect optical band gap may contribute to the broadening of the PL spectrum in bilayer $MoTe_2$. Overall, we conclude that emission from the direct optical band gap dominates the room temperature PL response of bilayer $MoTe_2$.

Third, the PL spectra of $N \geqslant 3$-layer $MoTe_2$ differ markedly from the mono- and bilayer cases. We observe (i) a broad and prominent PL^- feature (with a FHWM of approximately 100 meV), which, as N increases, progressively dominates the narrower PL^+ feature (with a FWHM in the range 60–70 meV), and (ii), as N increases, PL^-_{max} downshifts significantly, while PL^+_{max} remains almost constant and very close to the energy of the A exciton absorption line [27]. In the bulk limit, the PL^- peak is centered at 0.94 eV and is followed by a much fainter feature near 1.03 eV [55]. Thus, the PL^+ and PL^- peaks can tentatively be assigned to competing emission pathways, associated with hot luminescence from the

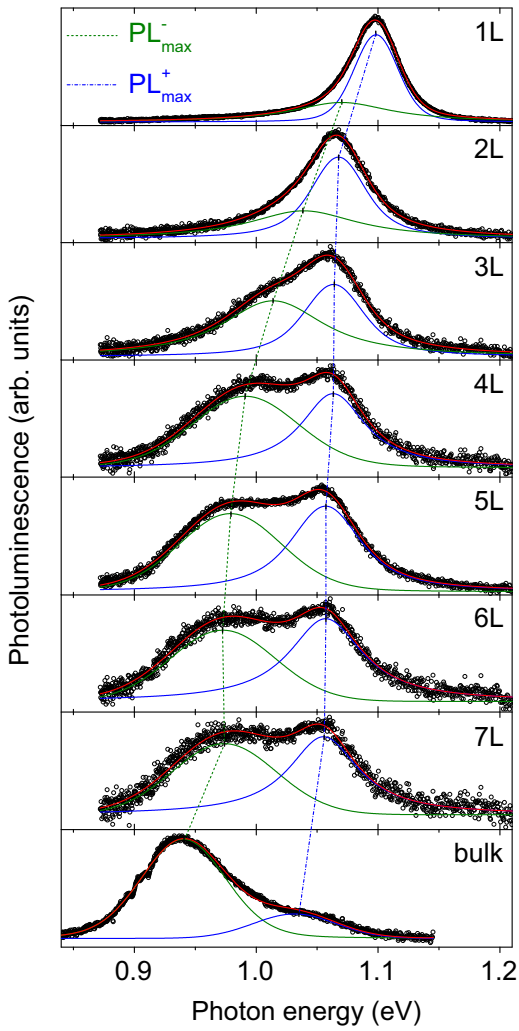

FIG. 3. Normalized interference-free photoluminescence spectra of $N = 1$ to $N = 7$ layer $MoTe_2$ and of bulk $MoTe_2$. The spectra are the same as in Fig. 2(b). The data (black open circles) are fit using the sum of two Voigt profiles (red solid lines). The green and blue solid lines are the PL^- and PL^+ features, respectively. The green dotted and blue dash-dotted lines mark the evolution of the associated peak energies, denoted PL^-_{max} and PL^+_{max}, respectively, as a function of the number of layers.

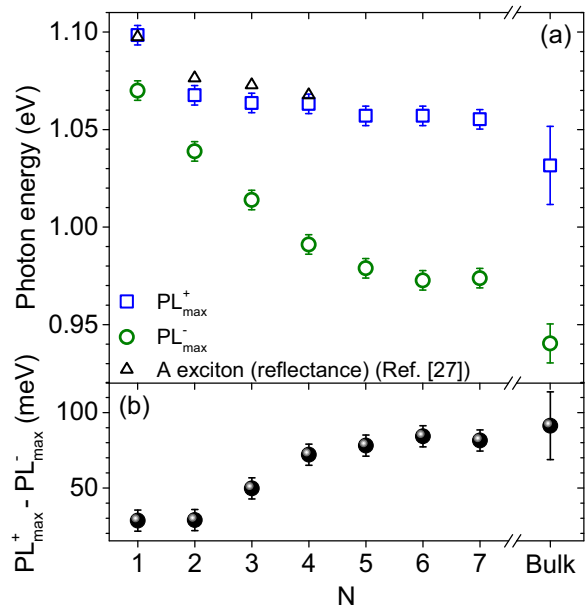

FIG. 4. (a) Energies of the photoluminescence peaks PL^-_{max} (green open circles) and PL^+_{max} (blue open circles) as a function of the number of layers N. The data are extracted from the fits, shown in Fig. 3 and correspond to the same samples as in Fig. 2(c). Our experimental measurements are compared to the reflectance measurements from Ref. [27] (open black triangles). (b) Energy difference between the two photoluminescence peaks as a function of the number of layers N.

A exciton and with phonon-assisted emission from the indirect excitons, respectively. Note that the PL^- peak is broader than the PL^+ peak, presumably due to the phonons involved in the indirect emission process. Finally, our conclusions are further confirmed by the fact that the bulk values of PL^+_{max} and PL^-_{max} are in fair agreement with previous measurements of the bulk direct and indirect optical band gaps obtained from optical transmission spectroscopy [24].

VI. EXCITON-EXCITON ANNIHILATION IN MONOLAYER $MoTe_2$

Having introduced monolayer $MoTe_2$ as a direct optical band gap semiconductor with bright near-infrared emission, we now focus on the influence of the exciton formation rate W_{abs} on its PL quantum yield and PL spectral line shape under cw laser excitation. W_{abs} is simply deduced from the *effective* absorptance of monolayer $MoTe_2$ in the air/$MoTe_2$/SiO_2/Si layered structure, by taking into account the size of our tightly focused laser spot, the absorptance of bare $MoTe_2$ [27], and optical interference effects (see Supplemental Material [53]). For a laser photon energy of 2.33 eV we calculated an absorptance of $\approx 16.5\%$ for monolayer $MoTe_2$ in our sample geometry. Assuming that one absorbed photon gives rise to one exciton, the exciton formation rates investigated here range from $W_{abs} \approx 1.0 \times 10^{19}$ up to 3.6×10^{22} $cm^{-2}\,s^{-1}$.

Figures 5(a) and 5(b) show PL spectra recorded on the same monolayer for increasing values of W_{abs}. The spectra have been normalized by the incoming laser intensity (i.e., by W_{abs}) and by the integration time. We clearly observe a nonlinear decrease of the *normalized* PL intensity that suggests, as shown in Fig. 5(c), that the *raw* integrated PL intensity levels off with increasing W_{abs}. We have checked that this nonlinear behavior was not due to irreversible photoinduced damage of the sample [31] and we have observed a very similar sublinear rise of the PL intensity on another $MoTe_2$ monolayer (see Supplemental Material [53]). As illustrated in Fig. 5(b), we notice that the linewidth of the PL spectra is independent of W_{abs} and that the PL spectra downshift very slightly (by only 3 meV) when W_{abs} reaches 3.6×10^{22} $cm^{-2}s^{-1}$ (i.e., a laser intensity of 81 kW/cm^2). We may thus conclude that biexciton emission [56] and photothermally induced modifications of the PL spectra can be neglected for the range of exciton densities explored here.

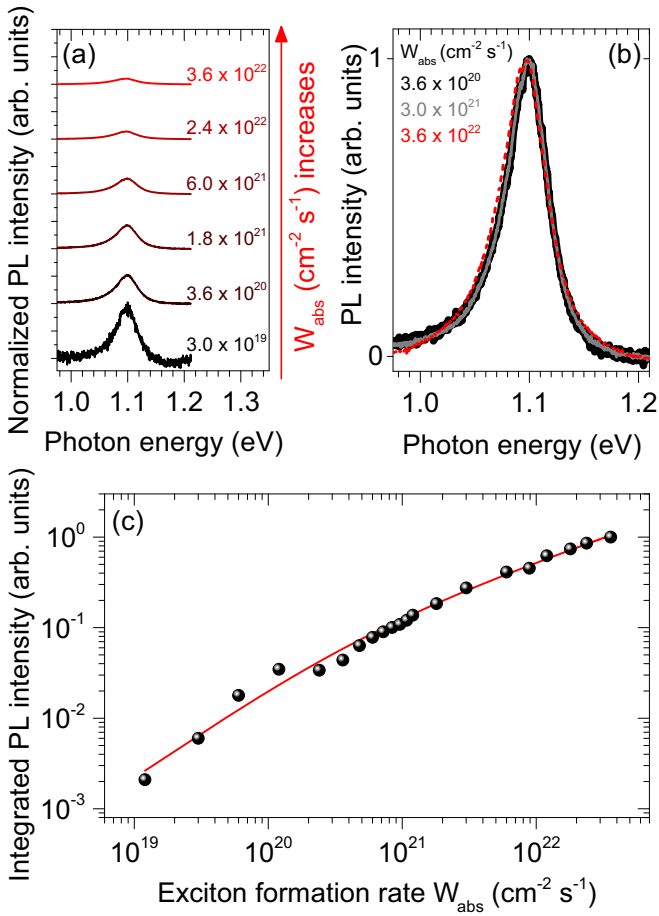

FIG. 5. (a) Photoluminescence spectra of a monolayer $MoTe_2$ sample at different exciton formation rates W_{abs}. The spectra are normalized using the product of W_{abs} by the integration time and vertically offset for clarity. (b) Photoluminescence spectra of monolayer $MoTe_2$ for three different exciton formation rates. The spectra have been normalized to unity. (c) Integrated photoluminescence intensity obtained from the raw spectra (symbols) as a function of W_{abs} in monolayer $MoTe_2$. The solid line corresponds to a fit based on Eq. (2). The error bars are smaller than the symbol size.

Sublinear rises of the integrated PL intensity, as observed in Fig. 5(c), have recently been reported in other MX_2 monolayers (such as WSe_2 [22,40,42], WS_2 [22,41,42], or MoS_2 [42]) and assigned to exciton-exciton annihilation (EEA). EEA has been further evidenced in these materials (and additionally in $MoSe_2$ [39]) by means of transient absorption spectroscopy [38,39,42] or time-resolved PL measurements [40,41] through the observation of accelerated exciton decays at high exciton densities. In order to further demonstrate our observation of EEA in monolayer $MoTe_2$, we make use of a simple rate equation model [42]. The integrated PL intensity is proportional to the steady state exciton density $\langle n_x \rangle$. Assuming that the time dependence of the exciton density n_x is essentially governed by the interplay between exciton formation (at a rate per unit area W_{abs}), linear recombination (at a rate Γ_x), and exciton-exciton annihilation (EEA) (at a rate γ_{eea}), one obtains

$$\frac{dn_x}{dt} = W_{abs} - \Gamma_x n_x - \gamma_{eea} n_x^2. \tag{1}$$

The EEA term in this equation scales quadratically with n_x since the annihilation process involves Coulomb interaction between two excitons. The steady state exciton density is

$$\langle n_x \rangle = \frac{\Gamma_x}{2\gamma_{eea}}\left(\sqrt{1 + \frac{4\gamma_{eea}}{\Gamma_x^2} W_{abs}} - 1\right). \tag{2}$$

The experimental data in Fig. 5(c) is very well fit by Eq. (2). From the fit we extract $\gamma_{eea}/\Gamma_x^2 \approx 1.4 \times 10^{-21}$ cm^2 s. Assuming a reasonable value of $\gamma_{eea} \sim 0.1$ cm^2 s^{-1}, similar to previous estimates in substrate-supported MX_2 monolayers [38–42], one obtains a linear exciton recombination rate of $\Gamma_x \sim 8.5 \times 10^9$ s^{-1}, that is a room temperature exciton lifetime of ~120 ps. Although additional near-infrared time-resolved measurements or transient absorption studies on monolayer $MoTe_2$ are needed to separately determine the exact values of γ_{eea} and Γ_x, our simple analysis provides values that are inline with recent room temperature measurements on other MX_2 [42,57]. Finally, let us also note that monolayer $MoTe_2$ and related systems exhibit EEA rates that give rise to average exciton decay times similar to those reported in carbon nanotubes [58,59] in the nonlinear regime. In addition, EEA in MX_2 is much more efficient than related processes (i.e., Auger recombination) in conventional quantum wells [38,60,61]. Highly efficient EEA between tightly bound excitons [15–22,62,63] in monolayer MX_2 reflects the strongly enhanced Coulomb interactions and reduced dielectric screening in these atomically thin two-dimensional materials.

VII. CONCLUSION AND OUTLOOK

We have performed a detailed analysis of the room temperature photoluminescence of N-layer $MoTe_2$. Monolayer $MoTe_2$ displays a direct optical band gap, with sharp emission at 1.10 eV. The crossover from a dominant direct excitonic emission (as observed in monolayers) to a dominant phonon-assisted indirect emission (in the bulk limit) occurs more smoothly than in other $2Hc$ transition metal dichalcogenides, such as MoS_2, $MoSe_2$, WS_2, and WSe_2. As a result, the difference between the bulk indirect optical band gap and the monolayer direct optical band gap is found to be only about 160 meV. Our observation of close-lying direct and indirect emission lines invites further calculations of exciton-phonon coupling in $MoTe_2$ and related systems, in order to correlate the values of the one-particle indirect band gap to the energy of the emission lines arising from indirect exciton recombination. Interestingly, in bilayer $MoTe_2$, the competition between direct and indirect emission may be efficiently manipulated by external electric fields [64–66], in particular using dual-gated field effect transistors. In addition, we have unveiled a sublinear scaling of the photoluminescence intensity of monolayer $MoTe_2$ with increasing exciton formation rate, which can be rationalized using a simple model based on exciton-exciton annihilation. This model also allowed us to obtain an order of magnitude estimate for the exciton lifetime in the linear regime that needs to be quantitatively confirmed by time-resolved photoluminescence measurements in the near-infrared range.

ACKNOWLEDGMENTS

We are grateful to L. Wirtz and A. Molina-Sánchez for stimulating discussions. We thank P. Bernhard at Roper Scientific for the loan of an InGaAs detector. We acknowledge financial support from the Agence Nationale de la Recherche (under grants QuanDoGra 12 JS10-001-01 and H2DH ANR-15-CE24-0016), from the LabEx NIE (under grant WHO), from the CNRS and from Université de Strasbourg.

[1] J. A. Wilson and A. D. Yoffe, The transition metal dichalcogenides discussion and interpretation of the observed optical, electrical and structural properties, Adv. Phys. **18**, 193 (1969).

[2] K. F. Mak, C. Lee, J. Hone, J. Shan, and T. F. Heinz, Atomically Thin MoS_2: A New Direct-Gap Semiconductor, Phys. Rev. Lett. **105**, 136805 (2010).

[3] A. Splendiani, L. Sun, Y. Zhang, T. Li, J. Kim, C.-Y. Chim, G. Galli, and F. Wang, Emerging photoluminescence in monolayer MoS_2, Nano Lett. **10**, 1271 (2010).

[4] C. Lee, H. Yan, L. E. Brus, T. F. Heinz, J. Hone, and S. Ryu, Anomalous lattice vibrations of single- and few-layer MoS_2, ACS Nano **4**, 2695 (2010).

[5] A. Molina-Sánchez and L. Wirtz, Phonons in single-layer and few-layer MoS_2 and WS_2, Phys. Rev. B **84**, 155413 (2011).

[6] G. Froehlicher, E. Lorchat, F. Fernique, C. Joshi, A. Molina-Sánchez, L. Wirtz, and S. Berciaud, Unified description of the optical phonon modes in N-layer $MoTe_2$, Nano Lett. **15**, 6481 (2015).

[7] Throughout the text, "direct optical band gap" and "indirect optical band gap" will thus denote the energy of the photons emitted from the direct and indirect band-edge excitons, respectively.

[8] S. Tongay, J. Zhou, C. Ataca, K. Lo, T. S. Matthews, J. Li, J. C. Grossman, and J. Wu, Thermally driven crossover from indirect toward direct bandgap in 2D semiconductors: $MoSe_2$ versus MoS_2, Nano Lett. **12**, 5576 (2012).

[9] P. Tonndorf, R. Schmidt, P. Böttger, X. Zhang, J. Börner, A. Liebig, M. Albrecht, C. Kloc, O. Gordan, D. R. T. Zahn, S. Michaelis de Vasconcellos, and R. Bratschitsch, Photoluminescence emission and Raman response of monolayer MoS_2, $MoSe_2$, and WSe_2, Opt. Express **21**, 4908 (2013).

[10] W. Zhao, Z. Ghorannevis, L. Chu, M. Toh, C. Kloc, P.-H. Tan, and G. Eda, Evolution of electronic structure in atomically thin sheets of WS_2 and WSe_2, ACS Nano **7**, 791 (2012).

[11] E. Cappelluti, R. Roldán, J. A. Silva-Guillén, P. Ordejón, and F. Guinea, Tight-binding model and direct-gap/indirect-gap transition in single-layer and multilayer MoS_2, Phys. Rev. B **88**, 075409 (2013).

[12] X. Xu, W. Yao, D. Xiao, and T. F. Heinz, Spin and pseudospins in layered transition metal dichalcogenides, Nat. Phys. **10**, 343 (2014).

[13] Q. H. Wang, K. Kalantar-Zadeh, A. Kis, J. N. Coleman, and M. S. Strano, Electronics and optoelectronics of two-dimensional transition metal dichalcogenides, Nat. Nanotechnol. **7**, 699 (2012).

[14] K. F. Mak, K. L. McGill, J. Park, and P. L. McEuen, The valley Hall effect in MoS_2 transistors, Science **344**, 1489 (2014).

[15] A. Molina-Sánchez, D. Sangalli, K. Hummer, A. Marini, and L. Wirtz, Effect of spin-orbit interaction on the optical spectra of single-layer, double-layer, and bulk MoS_2, Phys. Rev. B **88**, 045412 (2013).

[16] D. Y. Qiu, F. H. da Jornada, and S. G. Louie, Optical spectrum of MoS_2: Many-Body Effects and Diversity of Exciton States, Phys. Rev. Lett. **111**, 216805 (2013).

[17] A. Ramasubramaniam, Large excitonic effects in monolayers of molybdenum and tungsten dichalcogenides, Phys. Rev. B **86**, 115409 (2012).

[18] A. Chernikov, T. C. Berkelbach, H. M. Hill, A. Rigosi, Y. Li, O. B. Aslan, D. R. Reichman, M. S. Hybertsen, and T. F. Heinz, Exciton Binding Energy and Nonhydrogenic Rydberg Series in Monolayer WS_2, Phys. Rev. Lett. **113**, 076802 (2014).

[19] K. He, N. Kumar, L. Zhao, Z. Wang, K. F. Mak, H. Zhao, and J. Shan, Tightly Bound Excitons in Monolayer WSe_2, Phys. Rev. Lett. **113**, 026803 (2014).

[20] Z. Ye, T. Cao, K. OBrien, H. Zhu, X. Yin, Y. Wang, S. G. Louie, and X. Zhang, Probing excitonic dark states in single-layer tungsten disulphide, Nature (London) **513**, 214 (2014).

[21] G. Wang, X. Marie, I. Gerber, T. Amand, D. Lagarde, L. Bouet, M. Vidal, A. Balocchi, and B. Urbaszek, Giant Enhancement of the Optical Second-Harmonic Emission of WSe_2 Monolayers by Laser Excitation at Exciton Resonances, Phys. Rev. Lett. **114**, 097403 (2015).

[22] B. Zhu, X. Chen, and X. Cui, Exciton binding energy of monolayer WS_2, Sci. Rep. **5**, 9218 (2015).

[23] Y. Li, A. Chernikov, X. Zhang, A. Rigosi, H. M. Hill, A. M. van der Zande, D. A. Chenet, E.-M. Shih, J. Hone, and T. F. Heinz, Measurement of the optical dielectric function of monolayer transition-metal dichalcogenides: MoS_2, $MoSe_2$, WS_2, and WSe_2, Phys. Rev. B **90**, 205422 (2014).

[24] I. G. Lezama, A. Ubaldini, M. Longobardi, E. Giannini, C. Renner, A. B. Kuzmenko, and A. F. Morpurgo, Surface transport and band gap structure of exfoliated 2H-$MoTe_2$ crystals, 2D Mater. **1**, 021002 (2014).

[25] Y.-F. Lin, Y. Xu, S.-T. Wang, S.-L. Li, M. Yamamoto, A. Aparecido-Ferreira, W. Li, H. Sun, S. Nakaharai, W.-B. Jian, K. Ueno, and K. Tsukagoshi, Ambipolar $MoTe_2$ transistors and their applications in logic circuits, Adv. Mater. **26**, 3263 (2014).

[26] A. K. Geim and I. V. Grigorieva, van der Waals heterostructures, Nature (London) **499**, 419 (2013).

[27] C. Ruppert, O. B. Aslan, and T. F. Heinz, Optical properties and band gap of single- and few-layer $MoTe_2$ crystals, Nano Lett. **14**, 6231 (2014).

[28] I. G. Lezama, A. Arora, A. Ubaldini, C. Barreteau, E. Giannini, M. Potemski, and A. F. Morpurgo, Indirect-to-direct band gap crossover in few-layer $MoTe_2$, Nano Lett. **15**, 2336 (2015).

[29] J. Yang, T. Lu, Y. W. Myint, J. Pei, D. Macdonald, J.-C. Zheng, and Y. Lu, Robust excitons and trions in monolayer $MoTe_2$, ACS Nano **9**, 6603 (2015).

[30] M. Yamamoto, S. T. Wang, M. Ni, Y.-F. Lin, S.-L. Li, S. Aikawa, W.-B. Jian, K. Ueno, K. Wakabayashi, and K. Tsukagoshi, Strong enhancement of Raman scattering from a bulk-inactive vibrational mode in few-layer $MoTe_2$, ACS Nano **8**, 3895 (2014).

[31] B. Chen, H. Sahin, A. Suslu, L. Ding, M. I. Bertoni, F. M. Peeters, and S. Tongay, Environmental changes in $MoTe_2$ excitonic dynamics by defects-activated molecular interaction, ACS Nano **9**, 5326 (2015).

[32] S. Koirala, S. Mouri, Y. Miyauchi, and K. Matsuda, Homogeneous linewidth broadening and exciton dephasing mechanism in $MoTe_2$, Phys. Rev. B **93**, 075411 (2016).

[33] M. Kuiri, B. Chakraborty, A. Paul, S. Das, A. K. Sood, and A. Das, Enhancing photoresponsivity using $MoTe_2$-graphene vertical heterostructures, Appl. Phys. Lett. **108**, 063506 (2016).

[34] S. Tongay, H. Sahin, C. Ko, A. Luce, W. Fan, K. Liu, J. Zhou, Y.-S. Huang, C.-H. Ho, J. Yan, D. F. Ogletree, S. Aloni, J. Ji, S. Li, J. Li, F. M. Peeters, and J. Wu, Monolayer behavior in bulk ReS_2 due to electronic and vibrational decoupling, Nat. Commun. **5**, 3252 (2014).

[35] H. Zhao, J. Wu, H. Zhong, Q. Guo, X. Wang, F. Xia, L. Yang, P. Tan, and H. Wang, Interlayer interactions in anisotropic atomically thin rhenium diselenide, Nano Res. **8**, 3651 (2015).

[36] D. Wolverson, S. Crampin, A. S. Kazemi, A. Ilie, and S. J. Bending, Raman spectra of monolayer, few-layer, and bulk $ReSe_2$: An anisotropic layered semiconductor, ACS Nano **8**, 11154 (2014).

[37] E. Lorchat, G. Froehlicher, and S. Berciaud, Splitting of interlayer shear modes and photon energy dependent anisotropic raman response in N-layer $ReSe_2$ and ReS_2, ACS Nano **10**, 2752 (2016).

[38] D. Sun, Y. Rao, G. A. Reider, G. Chen, Y. You, L. Brzin, A. R. Harutyunyan, and T. F. Heinz, Observation of rapid exciton-exciton annihilation in monolayer molybdenum disulfide, Nano Lett. **14**, 5625 (2014).

[39] N. Kumar, Q. Cui, F. Ceballos, D. He, Y. Wang, and H. Zhao, Exciton-exciton annihilation in $MoSe_2$ monolayers, Phys. Rev. B **89**, 125427 (2014).

[40] S. Mouri, Y. Miyauchi, M. Toh, W. Zhao, G. Eda, and K. Matsuda, Nonlinear photoluminescence in atomically thin layered WSe_2 arising from diffusion-assisted exciton-exciton annihilation, Phys. Rev. B **90**, 155449 (2014).

[41] L. Yuan and L. Huang, Exciton dynamics and annihilation in WS_2 2D semiconductors, Nanoscale **7**, 7402 (2015).

[42] Y. Yu, Y. Yu, C. Xu, A. Barrette, K. Gundogdu, and L. Cao, Fundamental limits of exciton-exciton annihilation for light emission in transition metal dichalcogenide monolayers, Phys. Rev. B **93**, 201111 (2016).

[43] K. H. Michel and B. Verberck, Theory of rigid-plane phonon modes in layered crystals, Phys. Rev. B **85**, 094303 (2012).

[44] Y. Zhao, X. Luo, H. Li, J. Zhang, P. T. Araujo, C. K. Gan, J. Wu, H. Zhang, S. Y. Quek, M. S. Dresselhaus, and Q. Xiong, Interlayer breathing and shear modes in few-trilayer MoS_2 and WSe_2, Nano Lett. **13**, 1007 (2013).

[45] P. H. Tan, W. P. Han, W. J. Zhao, Z. H. Wu, K. Chang, H. Wang, Y. F. Wang, N. Bonini, N. Marzari, and N. Pugno, The shear mode of multilayer graphene, Nat. Mater. **11**, 294 (2012).

[46] X. Zhang, W. P. Han, J. B. Wu, S. Milana, Y. Lu, Q. Q. Li, A. C. Ferrari, and P. H. Tan, Raman spectroscopy of shear and layer breathing modes in multilayer MoS_2, Phys. Rev. B **87**, 115413 (2013).

[47] M. Boukhicha, M. Calandra, M.-A. Measson, O. Lancry, and A. Shukla, Anharmonic phonons in few-layer MoS_2: Raman spectroscopy of ultralow energy compression and shear modes, Phys. Rev. B **87**, 195316 (2013).

[48] M. Grzeszczyk, K. Goasa, M. Zinkiewicz, K. Nogajewski, M. R. Molas, M. Potemski, A. Wysmoek, and A. Babiski, Raman scattering of few-layers $MoTe_2$, 2D Mater. **3**, 025010 (2016).

[49] Q. J. Song, Q. H. Tan, X. Zhang, J. B. Wu, B. W. Sheng, Y. Wan, X. Q. Wang, L. Dai, and P. H. Tan, Physical origin of Davydov splitting and resonant Raman spectroscopy of Davydov components in multilayer $MoTe_2$, Phys. Rev. B **93**, 115409 (2016).

[50] D. Yoon, H. Moon, Y.-W. Son, J. S. Choi, B. H. Park, Y. H. Cha, Y. D. Kim, and H. Cheong, Interference effect on Raman spectrum of graphene on SiO_2/Si, Phys. Rev. B **80**, 125422 (2009).

[51] S.-L. Li, H. Miyazaki, H. Song, H. Kuramochi, S. Nakaharai, and K. Tsukagoshi, Quantitative Raman spectrum and reliable thickness identification for atomic layers on insulating substrates, ACS Nano **6**, 7381 (2012).

[52] M. Buscema, G. A Steele, H. S. J. van der Zant, and A. Castellanos-Gomez, The effect of the substrate on the Raman and photoluminescence emission of single-layer MoS_2, Nano Res. **7**, 561 (2014).

[53] See Supplemental Material at http://link.aps.org/supplemental/10.1103/PhysRevB.94.085429 for details on the calculation of the absorptance, optical interference effects, additional Raman scattering data, and additional photoluminescence data.

[54] C. Robert, R. Picard, D. Lagarde, G. Wang, J. P. Echeverry, F. Cadiz, P. Renucci, A. Högele, T. Amand, X. Marie *et al.*, Excitonic properties of semiconducting monolayer and bilayer $MoTe_2$, arXiv:1606.03337.

[55] Following Refs. [11,66] the difference between the values of the integrated PL intensities and of PL^{-}_{max} recorded in bulk and few-layer flakes ($N = 6,7$) (see Figs. 3 and 4) may arise from the fact that the bulk conduction band minimum occurs at a point in momentum space that lies halfway between the $\boldsymbol{K}$ and the $\boldsymbol{\Gamma}$ points, while the conduction band minimum is reached at the $\boldsymbol{\Gamma}$ point in the few-layer limit.

[56] Y. You, X.-X. Zhang, T. C. Berkelbach, M. S. Hybertsen, D. R. Reichman, and T. F. Heinz, Observation of biexcitons in monolayer WSe_2, Nat. Phys. **11**, 477 (2015).

[57] C. Robert, D. Lagarde, F. Cadiz, G. Wang, B. Lassagne, T. Amand, A. Balocchi, P. Renucci, S. Tongay, B. Urbaszek, and X. Marie, Exciton radiative lifetime in transition metal dichalcogenide monolayers, Phys. Rev. B **93**, 205423 (2016).

[58] Y.-Z. Ma, L. Valkunas, S. L. Dexheimer, S. M. Bachilo, and G. R. Fleming, Femtosecond Spectroscopy of Optical Excitations in Single-Walled Carbon Nanotubes: Evidence for Exciton-Exciton Annihilation, Phys. Rev. Lett. **94**, 157402 (2005).

[59] F. Wang, G. Dukovic, E. Knoesel, L. E. Brus, and T. F. Heinz, Observation of rapid Auger recombination in optically excited semiconducting carbon nanotubes, Phys. Rev. B **70**, 241403 (2004).

[60] A. Haug, Auger recombination in quantum well semiconductors: Calculation with realistic energy bands, Semicond. Sci. Technol. **7**, 1337 (1992).

[61] R. A. Taylor, R. A. Adams, J. F. Ryan, and R. M. Park, Exciton recombination dynamics in ZnCdSe/ZnSe quantum wells, J. Cryst. Growth **159**, 822 (1996).

[62] A. R. Klots, A. K. M. Newaz, B. Wang, D. Prasai, H. Krzyzanowska, J. Lin, D. Caudel, N. J. Ghimire, J. Yan, B. L. Ivanov, K. A. Velizhanin, A. Burger, D. G. Mandrus, N. H. Tolk, S. T. Pantelides, and K. I. Bolotin, Probing excitonic states in suspended two-dimensional semiconductors by photocurrent spectroscopy, Sci. Rep. **4**, 6608 (2014).

[63] M. M. Ugeda, A. J. Bradley, S.-F. Shi, F. H. da Jornada, Y. Zhang, D. Y. Qiu, W. Ruan, S.-K. Mo, Z. Hussain, Z.-X. Shen, F. Wang, S. G. Louie, and M. F. Crommie, Giant bandgap renormalization and excitonic effects in a monolayer transition metal dichalcogenide semiconductor, Nat. Mater. **13**, 1091 (2014).

[64] A. Ramasubramaniam, D. Naveh, and E. Towe, Tunable band gaps in bilayer transition-metal dichalcogenides, Phys. Rev. B **84**, 205325 (2011).

[65] N. Zibouche, P. Philipsen, A. Kuc, and T. Heine, Transition-metal dichalcogenide bilayers: Switching materials for spintronic and valleytronic applications, Phys. Rev. B **90**, 125440 (2014).

[66] T. Brumme, M. Calandra, and F. Mauri, First-principles theory of field-effect doping in transition-metal dichalcogenides: Structural properties, electronic structure, Hall coefficient, and electrical conductivity, Phys. Rev. B **91**, 155436 (2015).